Journal of Hazardous Materials 165 (2009) 332–344

Contents lists available at ScienceDirect

Journal of Hazardous Materials

journal homepage: www.elsevier.com/locate/jhazmat

An environmental screening model to assess the consequences to soil and groundwater from railroad-tank-car spills of light non-aqueous phase liquids

Hongkyu Yoon[a], Charles J. Werth[a,*], Christopher P.L. Barkan[a], David J. Schaeffer[b], Pooja Anand[a]

[a] Department of Civil and Environmental Engineering, University of Illinois at Urbana-Champaign, 205N Mathews Ave., Urbana, IL, United States
[b] Department of Veterinary Biosciences, University of Illinois at Urbana-Champaign, Urbana, IL, United States

ARTICLE INFO

Article history:
Received 9 January 2008
Received in revised form 7 July 2008
Accepted 30 September 2008
Available online 9 October 2008

Keywords:
NAPL
HSSM
Railroad-tank-car accident
Environmental consequence
Screening model
Hazardous materials transportation risk

ABSTRACT

North American railroads transport a wide variety of chemicals, chemical mixtures and solutions in railroad tank cars. In the event of an accident, these materials may be spilled and impact the environment. Among the chemicals commonly transported are a number of light non-aqueous phase liquids (LNAPLs). If these are spilled they can contaminate soil and groundwater and result in costly cleanups. Railroads need a means of objectively assessing the relative risk to the environment due to spills of these different materials. Environmental models are often used to determine the extent of contamination, and the associated environmental risks. For LNAPL spills, these models must account for NAPL infiltration and redistribution, NAPL dissolution and volatilization, and remediation systems such as pump and treat. This study presents the development and application of an environmental screening model to assess NAPL infiltration and redistribution in soils and groundwater, and to assess groundwater cleanup time using a pumping system. Model simulations use parameters and conditions representing LNAPL releases from railroad tank cars. To take into account unique features of railroad-tank-car spill sites, the hydrocarbon spill screening model (HSSM), which assumes a circular surface spill area and a circular NAPL lens, was modified to account for a rectangular spill area and corresponding lens shape at the groundwater table, as well as the effects of excavation and NAPL evaporation to the atmosphere. The modified HSSM was first used to simulate NAPL infiltration and redistribution. A NAPL dissolution and groundwater transport module, and a pumping system module were then implemented and used to simulate the effects of chemical properties, excavation, and free NAPL removal on NAPL redistribution and cleanup time. The amount of NAPL that reached the groundwater table was greater in coarse sand with high permeability than in fine sand or silt with lower permeabilities. Excavation can reduce the amount of NAPL that reaches the groundwater more effectively in lower permeability soils. The effect of chemical properties including vapor pressure and the ratio of density to viscosity become more important in fine sand and silt soil due to slow NAPL movement in the vadose zone. As expected, a pumping system was effective for high solubility chemicals, but it was not effective for low solubility chemicals due to rate-limited mass transfer by transverse dispersion and flow bypassing. Free NAPL removal can improve the removal efficiency for moderately low solubility chemicals like benzene, but cleanup times even after free NAPL removal can be prolonged for very low solubility chemicals like cyclohexane and styrene.

1. Introduction

North American railroads transport over 1000 different chemicals, chemical mixtures and solutions in railroad tank cars [1]. In the event of an accident, these materials may be spilled and impact soil and groundwater [2] and lead to costly cleanups [3]. Railroads need a means of objectively assessing the relative risk to the environment due to spills of these different materials [4]. Among the chemicals commonly transported are a number of water immiscible organic liquids, often referred to as non-aqueous phase liquids (NAPL). As spilled NAPLs migrate from the surface downward through the vadose zone, contaminant flow and transport occur in aqueous, gas, and NAPL phases. If NAPLs reach the groundwater table, then they will migrate further, both vertically and laterally depending upon their properties. As a consequence, NAPLs are present in both the vadose zone and groundwater and can act as a continuing source of groundwater contamination for long periods.

A number of sophisticated environmental models have been developed and successfully used to determine the extent of contamination and the associated environmental risks from spills of

* Corresponding author. Tel.: +1 217 333 3822; fax: +1 217 333 6968.
E-mail address: werth@uiuc.edu (C.J. Werth).

0304-3894/$ – see front matter © 2008 Elsevier B.V. All rights reserved.
doi:10.1016/j.jhazmat.2008.09.121

organic liquids. These models must account for NAPL infiltration and redistribution, dissolution and volatilization, and the effect of remediation systems such as pump and treat. However, for a variety of reasons the existing models are not suitable for practical, comparative assessment of the impact on soil and groundwater from the large number of different materials transported by rail. The environmental circumstances of the spill can vary widely depending on the location [2] and other conditions when the spill occurs. Also, certain characteristics typical of railroad-tank-car spills, such as size, spill rate and the shape of the initial surface pool of spilled material differ from those assumed by existing models. Therefore, a new model was needed to assess the risk to the environment due to rail transport of hazardous materials.

A quantitative environmental risk analysis of railroad transportation of hazardous materials was previously conducted by Barkan et al. [3]. In that study the probability of a spill was based on extensive statistical analysis of railroad accident rates and tank car safety performance in accidents. The environmental consequence analysis focused on a group of halogenated organic liquids that had caused particularly costly cleanups. The analysis did not consider many other materials such as LNAPLs that are transported by rail, nor did it account for variability in the possible environmental circumstances of a spill. Recently, Anand and Barkan [2] conducted a geographic information system (GIS) analysis of the railroad network to quantify the exposure of soil and groundwater to spills due to railroad accidents. Anand [4] extended this work by developing a comprehensive risk analysis model that quantitatively accounted for railroad accident probabilities, variation in tank car safety designs, hydrogeological features along rail lines and different chemical characteristics. However, the only environmental consequence model that was available in railroads [5] was based on work conducted in the 1980s and was not fully documented. Furthermore, it did not account for mechanistic NAPL movement and transport of dissolved chemicals in groundwater. In order to assess the environmental risk of soil and groundwater contamination due to transportation of hazardous materials, a model is needed that allows objective, quantitative comparison of the impact of spills under the variety of environmental conditions that most commonly occur along railroad lines.

Multiphase flow and transport models have been developed to address contamination and remediation in two-phase (aqueous-NAPL) and three-phase (aqueous-gas-NAPL) systems [6]. These models incorporate a variety of constitutive relations, and include interphase mass transfer processes, and coupling between transport and biological processes at a variety of scales. Several commonly used models include MISER [7], STOMP [8,9], TOUGH-2 [10,11], and UTCHEM [12]. Each of these numerically solves the requisite mathematical formulations in different ways. Unfortunately, these relatively sophisticated models require a large amount of chemical and hydrogeological data that are commonly not available at many spill sites nor in an emergency response time frame, and are computationally time intensive and expensive.

Several screening models have been developed as alternatives to multiphase flow and transport models. Screening models assume simplified conditions such as homogeneous permeability or simple layers of different permeability, a simple aquifer flow field, and constant parameters so that analytical and/or semi-analytical flow and transport models can be used to simulate the consequences of chemical spills in soil and groundwater. One of the most important assumptions used in a simple model of NAPL infiltration is to consider NAPL flow with constant or steady-state water saturation. Although there are many simple mathematical models describing single phase infiltration in the vadose zone [13], only a few deal with NAPL infiltration under a variety of boundary conditions and NAPL redistribution at the groundwater table. The Hydrocarbon Spill Screening Model (HSSM) [14–16] developed by the U.S. Environmental Protection Agency (EPA) is one such model; it has been used to estimate the effects of LNAPL spill volume and chemical properties on LNAPL redistribution in soils and groundwater, as well as down-gradient aqueous concentrations in the aquifer [17].

LNAPL that reaches groundwater typically forms a pool or lens at the groundwater table. A variety of simple mathematical models have been developed to describe dissolution of these pools and lenses into the water phase [18–20], and subsequent transport in groundwater [21,22]. Dissolution mechanisms often considered are mass transfer or equilibrium partitioning to the advecting pore water, and transverse dispersion from the NAPL source zone (DNAPL pool and LNAPL lens) to the surrounding water. The latter has been shown to limit the overall rate of dissolution and was evaluated by an analytical modeling analysis where the local equilibrium assumption was tested compared to the non-equilibrium mass transfer between the NAPL source zone and groundwater as well as experimental data [23]. The dispersive flux due to transverse dispersion from the NAPL source zone is considered in this work.

The objective of this paper is to develop a screening model to assess NAPL infiltration into soils and groundwater, and groundwater cleanup time using a pumping system. The effects of soil type, spill volume, excavation, and free NAPL removal on groundwater contamination and total cleanup time are considered. This work was motivated by an assessment of consequences of railroad-tank-car accidents to groundwater contamination and remediation, so model simulations use parameters and conditions representing typical characteristics along railroad lines. In particular, the HSSM, which assumes a circular spill area and a circular NAPL lens, was modified to account for a rectangular spill area (on the ground surface) and corresponding lens shape at the groundwater table, and for the effects of excavation and NAPL evaporation to the atmosphere. The modified HSSM was first used to simulate NAPL infiltration and redistribution. A NAPL dissolution and groundwater transport module developed in this work was then used to simulate the effects of chemical properties, excavation, and free (i.e., mobile) NAPL removal on NAPL redistribution and cleanup time. In all, six light non-aqueous phase liquids (LNAPL) commonly transported in railroad tank cars were evaluated. Implications of remediation efforts and cleanup times are discussed.

2. Model description

2.1. NAPL infiltration and redistribution module

A conceptual model of the processes considered is shown in Fig. 1. The HSSM accounts for one-dimensional vertical flow in the vadose zone and LNAPL redistribution in groundwater. Detailed discussions of the assumptions of the HSSM model have been published in the literature [14–16]. The environmental impact from a hazardous material spill due to the derailment of a railroad tank car depends on many factors including spill volume, spill area, limits of excavation, response and recovery time, chemical properties, and hydrogeological properties. When a chemical spill occurs on the ground surface, prompt removal of the spill product helps minimize health risk, environmental impacts, and potential damage to property and natural resources. Removal of ponded liquids and excavation of the contaminated soils can minimize soil and groundwater contamination. The shape of the spill area (i.e., ponded liquid) depends primarily on site topography and spill conditions (e.g., tank damage and spillage rate). Based on discussion with railroad environmental response experts it was concluded that a rectangular shape is more realistic than the circular shape used in the HSSM.

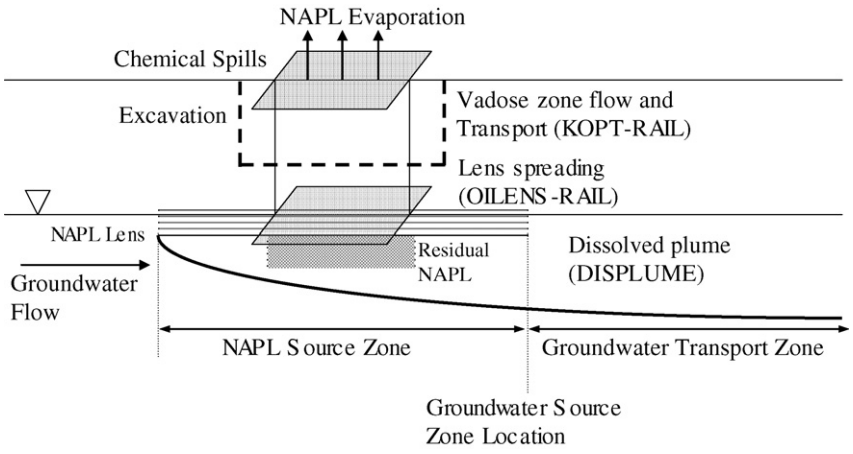

Fig. 1. Conceptual model of NAPL infiltration and redistribution.

This is due to the proximity of drainage ditches adjacent to railroad lines, where liquids often accumulate following a tank car spill. It is also not unusual to excavate and remove contaminated surface soil, so this factor also had to be accounted for in the modified HSSM.

A vadose zone flow and transport module (Kinematic Oily Pollutant Transport, KOPT) in the HSSM was modified (KOPT-RAIL) to account for the rectangular spill shape, excavation, and NAPL evaporation to the atmosphere. The change of the spill shape does not affect vertical NAPL flow in the vadose zone, but does affect LNAPL redistribution in groundwater. After excavation, the top boundary of the LNAPL plume in the vadose zone changes from the ground surface to the depth of excavation, assuming that LNAPL is completely removed by excavation to the depth of excavation. The maximum depth of excavation is currently 6 m or the depth to the groundwater table if less. The evaporation of a volatile liquid from a free-liquid surface to the atmosphere can affect the infiltration rate of liquids into soil. The evaporation rate of a liquid can be estimated by Kawamura and Mackay [24]

$$E = Ak_{\mathrm{m}}C_{\mathrm{g}} \tag{1}$$

where E is the evaporation rate (kg/s), A is the area of the evaporating liquid pool (i.e., spill area), k_{m} is the mass transfer coefficient (m/s), and C_{g} is the gas concentration of the liquid at the surface of the pool (kg/m^3), which can be computed using the vapor pressure and the ideal gas equation. An empirical equation for the mass transfer coefficient during liquid evaporation developed by MacKay and Matsugu [25] has been widely used, including for a NAPL spill case [26]:

$$k_{\mathrm{m}} = cSc^{-2/3}u^{7/9}x^{-1/9} \tag{2}$$

where c is a constant (0.0048) determined from experimental data, Sc is the Schmidt number, which is the ratio of the kinematic viscosity of air (1.5×10^{-5} m^2/s) to the molecular diffusivity of the compound in air (m^2/s), u is the wind speed at a height of 10 m (m/s), and x is the pool length in the wind direction (m). Eqs. (1) and (2) were added to the KOPT module in the HSSM.

The constitutive saturation–pressure–relative permeability (S–P–k) relation is a critical component of predictive multiphase flow models. In the residual NAPL formation theory developed by Lenhard et al. [27], the residual NAPL (i.e., NAPL held immobile by capillary forces) saturation in the vadose zone is not constant, but is estimated as a function of saturation-path history. The Brooks and Corey S–P model [28] with the Burdine relative permeability model is used in the HSSM. In the new k–S–P relation updated by [27], the relative permeability for NAPL becomes zero as the free (i.e., mobile) NAPL saturation becomes zero. Since residual NAPL is immobile, residual NAPL saturation does not contribute to NAPL relative permeability. This new NAPL relative permeability (k_{rn}) relation (Eq. (3)), including residual NAPL formation in the vadose zone [27], was added to the KOPT module as formulated below:

$$k_{\mathrm{rn}} = \left(\frac{S_{\mathrm{nf}}}{1-S_{\mathrm{wr}}}\right)^2 \left[\left(\frac{S_{\mathrm{w}}+S_{\mathrm{n}}-S_{\mathrm{wr}}}{1-S_{\mathrm{wr}}}\right)^{((2+\lambda)/\lambda)} - \left(\frac{S_{\mathrm{w}}+S_{\mathrm{gt}}-S_{\mathrm{wr}}}{1-S_{\mathrm{wr}}}+\frac{S_{\mathrm{nr}}}{1-S_{\mathrm{wr}}}\right)^{((2+\lambda)/\lambda)}\right] \tag{3}$$

where S_{n}, S_{nf}, and S_{nr} are the total NAPL, free NAPL, and residual NAPL saturations, respectively, S_{w} and S_{wr} are the total water and residual water saturations, respectively, S_{gt} is the trapped air saturation, and λ is the pore size distribution index. The maximum residual NAPL saturation can be observed after complete drainage of NAPL from a soil initially saturated with NAPL at the residual water saturation. In groundwater, the residual NAPL saturation in Eq. (3) was set to a constant value as used in the original HSSM.

If a chemical spill is large and infiltrates into soil fast enough to reach the groundwater table, and there is sufficient LNAPL head, LNAPL will displace water downward and then spread laterally to form a lens. The LNAPL distribution has two distinct regions after spreading is complete (Fig. 1). The first is a zone of residual LNAPL saturation that marks the region where LNAPL displaced groundwater downward before spreading outward to form a thin lens. The second is the thin LNAPL lens that eventually forms in the capillary fringe and on the groundwater table. The thickness of the lens was calculated with the Dupuit assumptions, where the flow is horizontal and the gradient is independent of depth. Since the shape of the spill area is rectangular instead of circular, the spreading of the lens is approximated by a rectangular shape in the x and y directions (i.e., cross shape) as shown in Fig. 2. Based on discussion with railroad environmental response experts it was also concluded that a rectangular shape of the lens is practically realistic. For practical purposes, the cross-shape of the lens predicted by the modified HSSM was converted to a rectangular shape. The outer portions of the lens in each direction (light gray parts in Fig. 2) were converted to the same area of the rectangle in the converted lens (dark gray parts in Fig. 2). NAPL thicknesses over the light gray area were averaged and the average NAPL thickness was distributed evenly over the dark gray area. The converted lens was used for NAPL mass transfer and dissolved plume development.

From the Dupuit equation and $h_{\mathrm{o}} = h_{\mathrm{os}}$ at $d = L_{\mathrm{s}}$ and $h_{\mathrm{o}} = 0$ at $d = L_t$ [29], the oil layer head (h_{o}) at any distance (d) along the x and y

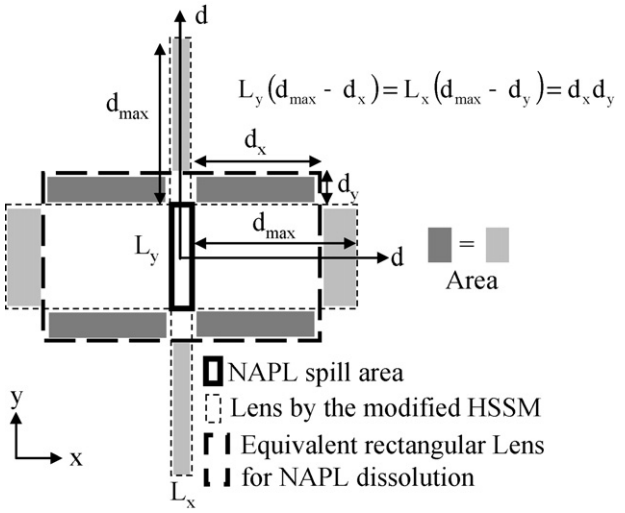

Fig. 2. Schematic of lens spreading and conversion to a rectangular lens.

directions outside the rectangular source area (i.e., spill area) is

$$h_o(d) = h_{os}\frac{\sqrt{L_t - d}}{\sqrt{L_t - L_s/2}} \tag{4}$$

where h_{os} is the lens oil head beneath the spill area, L_t is the length of the oil lens from the spill center at time t, and L_s is the size of the source area in the x and y directions (i.e., L_x and L_y). As seen in Eq. (4), the lens oil head depends on h_{os} and L_t. The rates of change of h_{os} and L_t can be obtained by applying the continuity principle to the control volumes of the lens beneath the spill area and the whole lens, respectively, as

$$\frac{dh_{os}}{dt} = \frac{1}{(L_x L_y)\theta_o \beta}(Q_{in} - Q_{spreading} - Q_{losses}) \tag{5}$$

$$\frac{dL_t}{dt} = \frac{Q_{in} - Q_{losses} - (\partial V_{TL}/\partial h_{os})(dh_{os}/dt)}{\partial V_{TL}/\partial L_t} \tag{6}$$

$$Q_{spreading} = -2L_y b_{os} K_o \left.\frac{dh_o}{dx}\right|_{x=Lx/2} - 2L_x b_{os} K_o \left.\frac{dh_o}{dy}\right|_{x=Ly/2} \tag{7}$$

where Q_{in} is the volumetric NAPL flow rate into groundwater from the vadose zone, Q_{losses} are the mass losses of the lens due to dissolution to groundwater, volatilization to the vadose zone, and the formation of residual (or trapped) NAPL as the lens height decreases, θ_o is an average effective volumetric NAPL content, β is a constant ($=\rho_w/(\rho_w - \rho_o)$), ρ_i is the density of phase i, b_{os} is the average lens thickness in the source area, K_o is the effective hydraulic conductivity of the LNAPL at θ_o, and V_{TL} is the total lens volume (i.e., $d = L_t$). The lens volume, V_L, as a function of distance (d) is

$$V_L(d) = L_x L_y \beta h_{os} + 2L_y \beta\theta_o h_{os}\left(\frac{2}{3}(L_t - L_x/2) - \frac{2}{3}\frac{(L_t - d)^{1.5}}{\sqrt{(L_t - L_x/2)}}\right) + 2L_x \beta\theta_o h_{os}\left(\frac{2}{3}(L_t - L_y/2) - \frac{2}{3}\frac{(L_t - d)^{1.5}}{\sqrt{(L_t - L_y/2)}}\right) \tag{8}$$

Eqs. (5) and (6) are a system of ordinary differential equations for the lens model and Eq. (8) is used to obtain the two derivatives in Eq. (6). The mass losses due to dissolution and volatilization can be computed using NAPL dissolution and volatilization module in the next section. The details of the derivation and numerical solution are provided in the HSSM Theory guide [16]. Eqs. (4)–(8) were added to the OILENS module in the HSSM (OILENS-RAIL) and all affected equations were also modified.

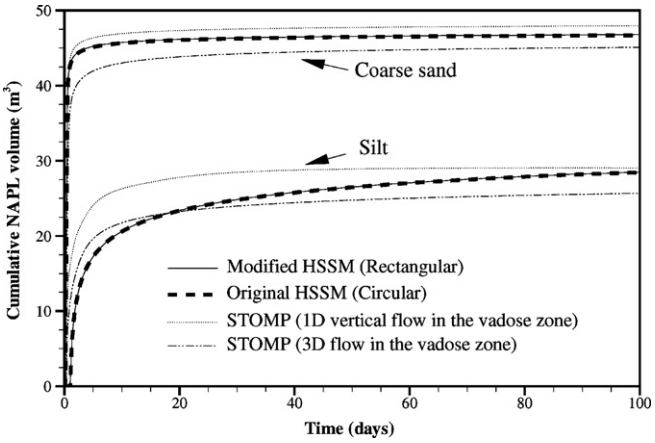

Fig. 3. Comparison of the cumulative NAPL volume across the capillary fringe.

The modified HSSM was compared to the original HSSM and a multiphase simulator, Subsurface Transport Over Multiple Phases (STOMP) [8,9]. For STOMP simulations, both 1D vertical NAPL flow and 3D NAPL flow in the vadose zone were considered, and 3D NAPL flow below the capillary fringe was considered. For a typical LNAPL (i.e., benzene) spilled in homogeneous coarse sand and silt considered in this study, cumulative LNAPL volume across the capillary fringe and the NAPL lens area for a 50% spill case (i.e., 50% of a tank car volume) without excavation are shown in Figs. 3 and 4. The

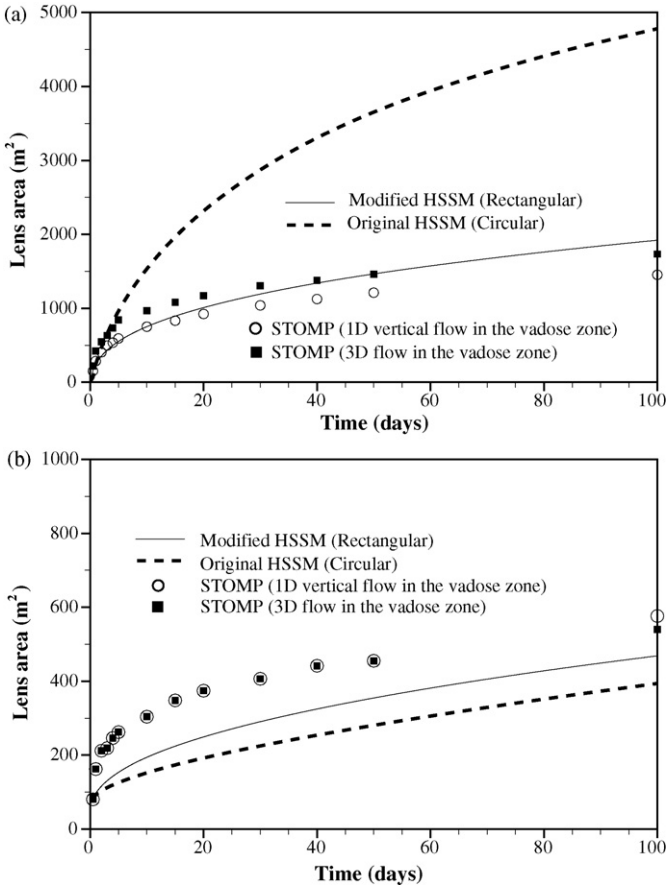

Fig. 4. Comparison of the lens area in (a) coarse sand and (b) silt.

original HSSM assumed a circular LNAPL pool shape at the ground surface whereas the modified HSSM and STOMP assume a rectangular shape. The comparison of the cumulative NAPL volumes across the capillary fringe in Fig. 3 showed that in two different soils the NAPL volume in the modified HSSM was almost identical to that in the original HSSM and within the range of STOMP results between 3D and 1D NAPL flow in the vadose zone. The comparison of the lens area in Fig. 4 showed that the modified HSSM predicted the lens area well within the range of STOMP prediction in coarse sand and 20% lower than that of STOMP prediction in silt. However, the original HSSM over-predicted and under-predict the lens area, compared to STOMP results in coarse sand and silt, respectively. The main reason for the under-prediction of the modified HSSM in the silt compared to the STOMP is that in the silt LNAPL can spread above the capillary fringe (i.e., unsaturated soil) in the STOMP simulation, while the modified HSSM considers NAPL flow only in the saturated zone. This difference decreased with increasing permeability because LNAPL can penetrate through the capillary fringe more easily with increasing permeability, resulting in less spreading above the capillary fringe. This comparison indicates that the modified HSSM adequately captures the physics that govern LNAPL migration and lens formation.

2.2. NAPL dissolution and volatilization module

Mass transfer from the LNAPL source zone (i.e., LNAPL lens and residual LNAPL) is influenced by a variety of factors including LNAPL properties, the size of the LNAPL lens and residual region, and the heterogeneity of porous media. The LNAPL lens in direct contact with the water and gas phases undergoes dissolution and volatilization (Fig. 5). Residual LNAPL located below the LNAPL lens undergoes only dissolution. Rate-limited NAPL dissolution has been observed at high water velocities and low NAPL saturation. Many studies have used a first-order mass transfer model to quantify this process; experimental and numerical results are summarized in literature [6,19,20,23,30]. Despite numerous investigations, it is not clear how to quantify NAPL dissolution rates in the field. In this work, we modified the approach proposed by Falta [20] and considered four components of NAPL mass flux from the source zone: advective flux from groundwater flow, dispersive flux in the y direction, dispersive flux in the z direction, and diffusive flux in the gas phase toward the ground surface from the LNAPL lens.

The dissolved concentration within the LNAPL source zone is assumed to be in equilibrium with the NAPL phase; hence the dissolved concentration is the aqueous solubility of the chemical. This follows from earlier work [23], where local equilibrium within a NAPL source zone was found to adequately describe the concentration driving force for dispersion under similar conditions. The advective flux through the LNAPL source (lens and residual), J_{adv}, is simply the product of the water specific discharge (q) and the solubility (C_{sol});

$$J_{adv} = qC_{sol} \tag{9}$$

The groundwater specific discharge varies as a function of water saturation:

$$q_w = -\frac{k_{rw}k\rho_w g}{\mu_w} i \tag{10}$$

where k_{rw} is the water relative permeability, k is the intrinsic permeability of the soil, ρ_w is the water density, g is the gravitational constant, μ_w is the water viscosity, and i is the hydraulic gradient. The Brooks-Corey saturation–capillary pressure (S–P) model with the Burdine relative permeability model (BCB model) and the van-Genuchten S–P model with the Mualem relative permeability model (VGM model) were used. Fluid entrapment and hysteresis were not considered due to complexity. The BCB model considers a distinct nonwetting fluid entry pressure. The water relative permeability, k_{rw}, is given by:

$$k_{rw} = \left(\frac{S_w - S_{wr}}{1 - S_{wr}}\right)^{((2+3\lambda)/\lambda)} \tag{11}$$

where the water saturation, S_w, is simply $(1 - S_n)$.

The dissolved chemical concentration from the LNAPL source zone in the z direction is given by the steady-state dispersion equation as developed by [31]:

$$v\frac{\partial C}{\partial x} = D_t\frac{\partial^2 C}{\partial z_t^2} \text{ with } C = C_{in} \text{ at } x = 0,\ C = C_{sol} \text{ at } z_t = 0,$$
$$C = 0 \text{ at } z_t \to \infty \tag{12}$$

where v is the water pore velocity, D_t is the transverse dispersion coefficient, C_{in} is the influent dissolved chemical concentration, x is the distance of the NAPL source zone along the groundwater flow direction, and z_t are the transverse distance in the z direction from the NAPL source zone. The hydrodynamic dispersion coefficient is given by:

$$D_t = D_{eff} + v\alpha_t \tag{13}$$

where D_{eff} is the effective diffusion coefficient and α_t is the transverse dispersivity in the z direction. The effective diffusion coefficient is the product of the tortuosity, which is simply porosity in this study, and the aqueous diffusion coefficient. The solution to Eq. (12) is

$$C(L_x, z_t) = C_{in} + (C_{sol} - C_{in})erfc\left(\frac{z_t}{2\sqrt{D_t L_x/v}}\right) \tag{14}$$

where L_x is the horizontal distance along the LNAPL source zone. The same approach is considered in the y direction. The total mass flux from each direction can be obtained by integrating the concentration with respect to z and y:

$$J_{disp} = (C_{sat} - C_{in})\phi\sqrt{4D_t v L_x/\pi} \tag{15}$$

The NAPL dissolution processes implemented in this study were tested against a three-dimensional NAPL dissolution data set [32]. Comparison of simulated and experimental average effluent flux at the end of the 3D sandbox showed that among four cases, average percent error in the two best cases was less than 5% and in one case was less than 25%, and total NAPL removal time was predicted accurately (i.e., within 6%) [32].

LNAPL in direct contact with the gas phase is depleted by NAPL volatilization. NAPL volatilization is described using Fick's First Law for steady-state vapor transport toward the ground surface with a zero concentration boundary:

$$J_v = -D_{veff}\frac{dC}{dz} = D_{veff}\frac{C_{vsat}}{Z_{depth}} \tag{16}$$

where J_v is the vapor diffusive flux from the top of the LNAPL to the ground surface, D_{veff} is the effective vapor diffusion coefficient, C_{vsat} is the saturated gas concentration, and Z_{depth} is the distance from the top of the LNAPL to the ground surface. D_{veff} is computed using the Millington and Quirk [33] equation.

In this work, a simplified 3D source geometry was used to accommodate the variety of LNAPL distributions that result from the modified HSSM. The continuous LNAPL distribution was converted into a discrete 3D geometry by volumetric averaging. The two distinct NAPL source zones (i.e., lens and residual zones) were averaged differently. First, the LNAPL lens was averaged into two layers, in which NAPL saturations were volumetric average saturations above and below the groundwater table. The LNAPL lens

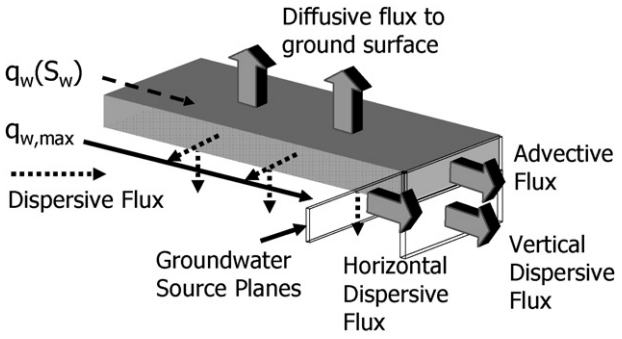

Fig. 5. Schematic of four different NAPL dissolution and volatilization processes. Schematic shows half of the LNAPL source zone by symmetry along the main flow direction.

thickness decreased with increasing distance from the center of the LNAPL source, resulting in varying LNAPL saturation over distance. The scale of a grid block was 0.5 m × 0.5 m in the horizontal direction and varied in the vertical direction depending upon the LNAPL lens thickness. Second, the length of residual NAPL was calculated based upon a threshold saturation below which no residual NAPL exists. Since in most cases the residual NAPL zone was located below the center of the NAPL source, the residual NAPL zone was considered as a rectangular shape (Fig. 1). The vertical grid in the area of residual NAPL (i.e., below the LNAPL lens) was 0.02 m. The grid spacing can be easily adjusted.

Semi-analytical solutions that update the size of the source area and NAPL saturation over time are used to reduce computational time as follows. First, NAPL dissolution due to the advecting water through a grid block occurs within the first grid block upgradient along the groundwater flow direction, but there is no net NAPL dissolution by advection through the remaining grid blocks downgradient. Second, the dispersive flux in the z and y directions (Eq. (15)) is updated in two regions: the dispersive flux from the first grid block upgradient is used to revise the NAPL saturation in the block. The NAPL saturations in the rest of the NAPL blocks downgradient are updated based on the average dispersive flux, which is the difference between the total dispersive flux along the entire length of the LNAPL source zone and the average dispersive flux from the upgradient grid block(s). As a result, NAPL is removed first from the upgradient block of the source zone advectively, and from the bottom and the side of the source zone dispersively. Finally, the diffusive flux (Eq. (16)) due to NAPL volatilization from the LNAPL lens is computed (Fig. 5).

2.3. Contaminant transport module

The end of the LNAPL source zone serves as the source plane of the dissolved chemical transport zone (Fig. 1). The Domenico [34] solution with Martin-Hayden and Robbins [35] improvements and first-order biodegradation implemented in BIOCHLOR [36] (referred in this work as the "modified Domenico model") was used to calculate downgradient dissolved contaminant concentrations; it considers advection, dispersion, linear sorption, an exponentially decaying source boundary condition, and first-order biodegradation in the aqueous phase. The original Domenico model was derived for a single planar source of constant concentration. In this work, the Domenico model was modified by superimposing the Domenico solution over multiple source areas as a function of time (Fig. 6). As the NAPL source zone configuration changed due to dissolution and volatilization, the transient solution for the concentrations over multiple source areas was computed using the NAPL dissolution and volatilization module. The concentrations at the source planes were computed by considering the total mass flux due to advection and dispersion divided by the average flow rate. The number of source planes can be easily adjusted. The accuracy of the modified Domenico solution implemented in this work was compared against the exact semi-analytical solution for the 3D transport problem using a program PATCHI in Wexler [37]. The results in this work showed good agreement with those from Wexler [37] as shown in Fig. 6. As described in considerable detail in several recent reviews [38–40], the accuracy of the Domenico model depends mostly upon the value of longitudinal dispersivity and the position of the advective front of the plume. Since the problems presented in this study consider relatively short groundwater plumes because cleanup begins quickly after a spill occurs (e.g., 30 days), the modified Domenico model can be used because longitudinal dispersivity is small due to the short distance of the contamination plume.

2.4. Pumping module

Two different pumping systems were used to remove the NAPL source zone and capture contaminated groundwater plume, respectively (Fig. 6). For NAPL source zone removal, the pumping system is located downgradient from the NAPL source zone. The location of pumping wells is determined by minimizing the number of pumping wells and capturing the entire NAPL source zone. The pumping system for capturing the groundwater plume is located downgradient from that for NAPL source zone removal. Hence, two pumping systems are separated by a water divide. For both

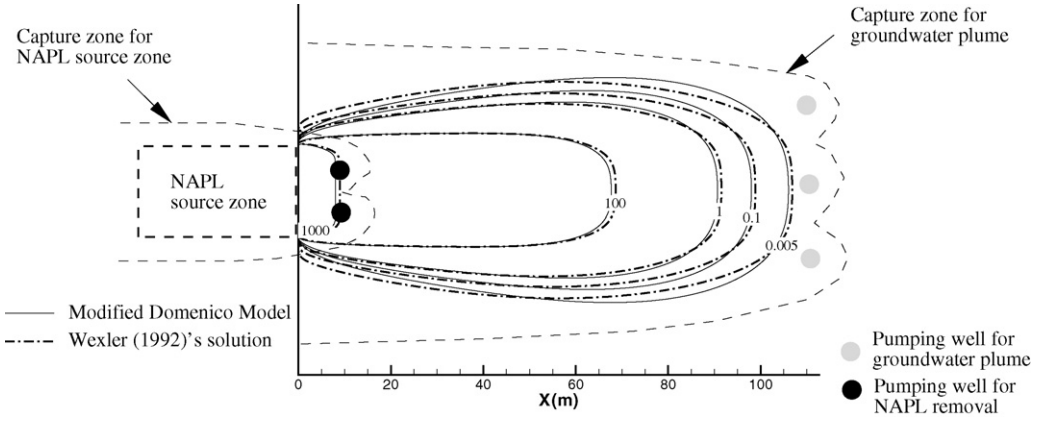

Fig. 6. Plan view of pumping systems for NAPL removal and capturing dissolved plume. Comparison of the modified Domenico model and Wexler (1992)'s solution is shown. Parameters for coarse sand in Table 2 were used.

Table 1
Chemical properties used in simulations[a].

Chemicals	Density (kg/L)	Viscosity (cp)	NAPL water interfacial tension (dyne/cm)	Water surface tension (dyne/cm)	Solubility (mg/L)	Vapor Pressure (atm)	Diffusion coefficient in gas (cm^2/s)
Acrylonitrile	0.801	0.35	10.38[1]	50.5[1]	7.45E+04	0.072	0.106
Benzene	0.877	0.604	35	60.6	1.78E+03	0.0846	0.09
Cyclohexane	0.774	0.894	50.0	72.0	5.50E+01	0.0803	0.074
MTBE	0.735	0.333	10.5[2]	30.5[2]	5.00E+04	0.217	0.075
Styrene	0.902	0.695	32.5	62.5	3.10E+02	0.0059	0.071
Vinyl acetate	0.926	0.421	30.0	54.0	2.30E+04	0.11	0.085

Density and viscosity were from the Hazardous Substances Data Bank (HSDB) [50]. NAPL-water interfacial tension and water surface tension were from Demond and Lindner [51] and HSDB [50]. Solubility and diffusion coefficient in gas were from U.S. EPA [52]. Vapor pressure was from Ohe [53] and HSDB [50]. [1]These data are based upon the properties of butyronitrile in Demond and Lindner [51]. [2]From Hickel et al. [54] and water surface tension is computed by assuming a zero spreading coefficient.
[a] All data were in the range of 20–25 °C except for saturated gas concentration at 15 °C.

pumping systems, the domain is assumed to be homogeneous, isotropic, and with constant groundwater flow. For an unconfined aquifer with the fully penetrated pumping well, the Dupuit assumption (i.e., vertical gradients are negligible) is commonly used in analytical groundwater modeling [29,41,42]. Recently, the effect of the drawdown in an unconfined aquifer (i.e., variation of water table) on the travel time to a pumping well was compared to that in a confined aquifer [42]. For an aquifer thickness of 10 m considered in this study and a drawdown of 2 m at the well, the error for ignoring the effect of the drawdown was less than 10% [42]. As indicated in [42], the effect of the vertical flow needs to be tested if the ratio of the drawdown to the aquifer thickness is greater than 0.5.

The number of pumping wells for two pumping systems was separately computed. The number of NAPL source zone removal wells was computed by dividing the width of the NAPL source zone by the minimum width of a single well capture zone. The number of wells for capturing the plume was computed similarly by dividing the plume width by the width of a single well capture zone. For low solubility chemicals, the NAPL removal time is expected to be much longer than the time required to capture the plume. Hence, only the pumping system for NAPL source zone removal is operated after all the dissolved plume is captured. For NAPL source zone removal, no NAPL flow is assumed. If NAPL flow is expected to be significant, free-product removal can be used before pumping. The effect of free NAPL removal on cleanup time was tested in Section 4. It was assumed that all remaining NAPL in the vadose zone was removed by soil excavation or soil vapor extraction when pumping begins. Hence, NAPL in the vadose zone is not considered a long-term source of groundwater contamination after pumping. NAPL removal processes during pumping are the same as described in the previous section, only the groundwater flow velocity (v) in Eqs. (13)–(15) is different. The groundwater flow velocity components V_x and V_y in the x and y directions, respectively, are given by [41,43]:

$$V_x = \frac{q}{\phi} + \frac{Q_w x}{2\pi\phi B(x^2+y^2)} \tag{17}$$

$$V_y = \frac{Q_w y}{2\pi\phi B(x^2+y^2)} \tag{18}$$

$$v = \sqrt{V_x^2 + V_y^2} \tag{19}$$

where Q_w is the rate of pumping, B is the aquifer thickness, x and y are the distances to the pumping well. For capturing the groundwater plume, a model using the concept of arrival distribution time [44] was chosen for this study. The details of the method are available in Kinzelbach [45]. The time required to capture the contaminant plume is the travel time of the contaminant from the outer boundary of the plume to the pumping well and is calculated as [45]

$$t_{plume} = \frac{\phi Q_w R}{2\pi v^2 B}\left(L\frac{2\pi vB}{Q_w} - \ln\left(L\frac{2\pi vB}{Q_w}+1\right)\right) \tag{20}$$

where R is the retardation factor, and L is the distance to the pumping well.

3. Example problems

Six LNAPLs frequently shipped in railroad tank cars were used to illustrate the effects of chemical properties on cleanup (Table 1). The hydrogeological properties and transport parameters of three soil types, coarse sand, fine sand, and silt, were considered (Table 2). The modeling domain was assumed to be homogeneous and isotropic and all parameters used in this study were assumed to be constant over time. Four depths to groundwater, 3, 6, 15, and 30 m, were used in the simulations. These depths were chosen to span the most common depths identified from a U.S. Geological Survey (USGS) dataset of the groundwater depth in the U.S. [46]. Water saturation in the vadose zone is assumed at residual water saturation.

The spill volume in a tank car accident can vary from a few liters to the entire tank car contents. The maximum amount spilled is also affected by the volumetric capacity of the tank car, which varies depending on the density of product it is intended to transport. The capacity of most North American tank cars ranges from about 45,000 to over 115,000 L. The distribution of spill amounts from tank cars in mainline accidents can be considered in terms of percentage tank capacity lost in a release accident [47]. For this study we used the percentage categories, 0–5%, 5–20%, 20–80%, and 80–100% and assumed the arithmetic mean quantity spilled for

Table 2
Soil properties used in simulations.

Physical properties	Coarse sand	Fine sand	Silt
Hydraulic conductivity (m/d)	50	7	1
Hydraulic gradient	0.006	0.006	0.006
Pore size distribution index	1.5	0.5	0.5
Air entry pressure (m)	0.15	0.3	0.5
Residual water saturation	0.048	0.1	0.2
Maximum residual NAPL saturation in the vadose zone	0.03	0.05	0.10
Residual NAPL saturation in groundwater	0.1	0.1	0.1
Lens NAPL saturation	0.35	0.35	0.35
Effective porosity	0.42	0.33	0.33
Horizontal transverse dispersivity in the NAPL source (m)	0.05	0.05	0.05
Vertical transverse dispersivity in the NAPL source (m)	0.025	0.025	0.025
Longitudinal dispersivity (m)	1	1	1
Transverse dispersivity (m)	0.1	0.1	0.1

Table 3
Input parameters used in simulations.

Condition			Value assumed	
Size of a tank car (m^3)			99.30	
Spill duration (hrs)			12	
Maximum depth of excavation (m)			6	
Excavation time (days)			4	
Remediation time (days)			30	
Aquifer thickness (m)			10	
Soil-type-specific conditions		Coarse sand	Fine sand	Silt
Spill length (m), L_x		1.5	3.0	4.5
Spill width (m), L_y	2.5% spill	3	3	4.5
	12.5% spill	6	6	12
	50% spill	16.7	16.7	30.5
	90% spill	30	30	61
Pumping rate (m^3/d)		200	200	20

For 50% and 90% spill cases, infiltration rate (=spill volume/spill area/spill duration) was almost the same.

each respective category as follows, 2.5%, 12.5%, 50%, and 90%. In this study we assumed a tank volume of 99.3 m^3, a size typical of tank cars used for many NAPLs. A variety of other assumptions also had to be made for purposes of comparison (Table 3). It was assumed that all spill volumes, except for the fraction of NAPL that evaporates, infiltrate into the soil. The spill width was determined based on expert opinion and actual accident records [4]. The spill area was determined based on the spill width and volume and run-off over the ground surface was not considered. Groundwater remediation was assumed to begin 30 days after the spill based on anticipated response times for cleanup by railroad personnel.

Unless otherwise stated, excavation was assumed complete four days after the spill occurred, and the maximum excavation depth was six m. We also compared the effect of no excavation and excavation after only two days. The effect of free NAPL recovery on cleanup time for low solubility chemicals was also investigated. In this study, no module was developed for free NAPL recovery. Instead, all mobile NAPL was removed before pumping in order to evaluate the effect on cleanup time; hence remaining NAPL was set to a residual NAPL saturation. The importance of free NAPL recovery highlights the importance of using free-product recovery at real field sites. Since remediation was assumed to start within a month, for low solubility chemicals the contaminant plume did not move far from the NAPL source zone and thus a few pumping wells can capture the plume down gradient. For high solubility chemicals (>10,000 mg/L) a pumping rate of 20 m^3/d was used since preliminary tests showed this pumping rate is enough to capture the contaminant plume. The number of pumping wells and pumping time required to remove the contaminant plume and NAPL source zone were computed. For the purposes of this paper, groundwater cleanup time by the pumping well system was computed for the NAPL source zone and the contaminant plume.

4. Results and discussion

4.1. NAPL volume in groundwater

The NAPL volume that reached groundwater for the six chemicals was calculated at 30 days after the spill occurred (Fig. 7). The NAPL saturation was close to one near the ground surface in most cases. A sharp front of constant NAPL saturation migrated downward until the NAPL pool at the ground surface was depleted. After this, the NAPL saturation decreased as the NAPL front continued to migrate downward, and residual NAPL was left behind trapped in the pore space. The NAPL relative permeability decreased with

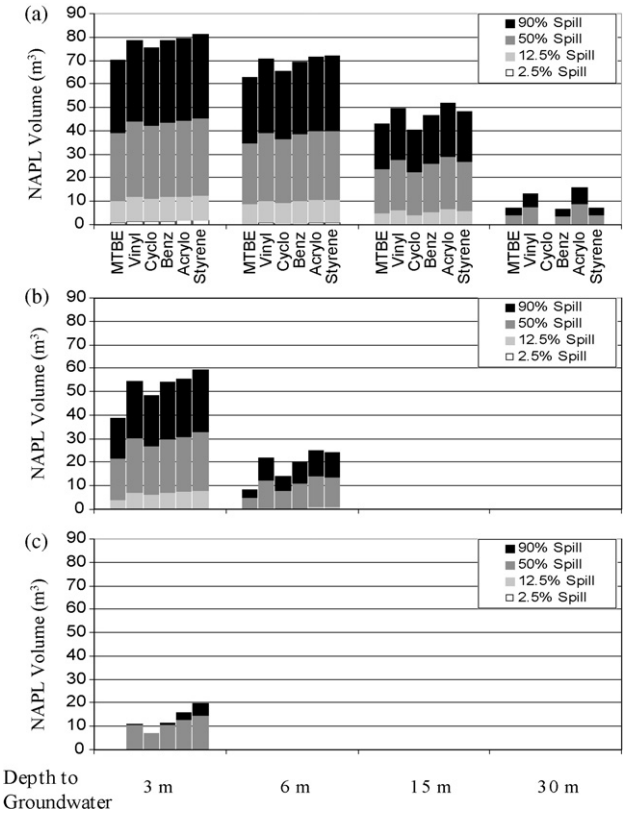

Fig. 7. NAPL amounts across the capillary fringe in (a) coarse sand, (b) fine sand, and (c) silt. The percentage represents the percentage spill of a tank car volume (99.1 m^3). The end of each bar represents NAPL volume across the capillary fringe. Six chemicals are acrylonitrile (Acryl), vinyl acetate (Vinyl), MTBE (MTB), benzene (Benz), styrene (Styre), and cyclohexane (Cyclo).

decreasing NAPL saturation, resulting in slower NAPL migration with time. If the spilled NAPL volume and migration rate were sufficiently large, a portion of the spilled NAPL reached groundwater.

The six chemicals considered in this study have vapor pressures ranging from 0.0059 to 0.217 atm, and density to viscosity ratios ranging from 0.8 to 2.3 kg/L/cP. The chemicals are presented in Fig. 7 from left to right in order of decreasing vapor pressure. NAPL amounts that reached groundwater increase with decreasing vapor pressure for groundwater depths up to six m with the exception of vinyl acetate due to its high density to viscosity ratio. The total amount of NAPL that evaporates to the atmosphere is proportional to the spill area (Eq. (1)). The more NAPL mass that evaporates, the less NAPL mass that infiltrates into soils, particularly, in silt because it has a larger spill area than the other soils due to its lower permeability (Table 2). For example, NAPL evaporation into the atmosphere for MTBE accounted for approximately 12%, 24%, and 48% of the total spill amount for a 90% spill case in the coarse sand, fine sand, and silt, respectively. The effect of NAPL evaporation for benzene, acrylonitrile, and styrene was not significant due to the short period of the NAPL spill (12 h) and the lower vapor pressures of these compounds (Table 1). Acrylonitrile, vinyl acetate, and MTBE have ratios of density to viscosity within 5%; NAPL amounts that reached groundwater were very similar for vinyl acetate and acrylonitrile at all depths, but the NAPL amount was smaller for MTBE, mainly due to its high vapor pressure. Except for MTBE with the highest vapor pressure and for styrene with the lowest vapor pressure, the NAPL amount that reached groundwater increased with increasing values of the density to viscosity ratio for all groundwater depths and in all soils (Fig. 7).

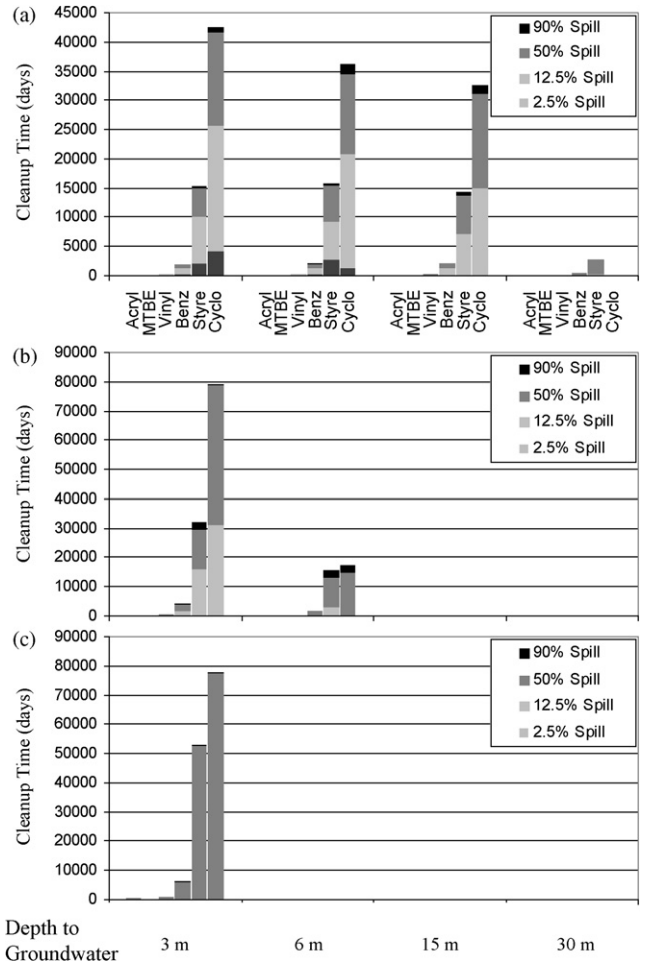

Fig. 8. Groundwater cleanup time with a pumping system in (a) coarse sand, (b) fine sand, and (c) silt.

The permeability in the coarse sand is 50 times higher than silt (Table 2). As expected, the NAPL amount that reaches groundwater decreases with decreasing soil permeability, but the decrease is not linearly proportional to the decrease in the permeability. This is mainly due to the effect of excavation on the amount of free NAPL. For example, a large portion of NAPL reached groundwater at a depth of 3 m in the coarse and fine sands before excavation was performed. Since the maximum depth of excavation was 6 m, all NAPL remaining in the vadose zone above this was removed after four days. Hence, the amount of NAPL that reached groundwater decreased dramatically for groundwater depths deeper than six m in the fine sand compared to the coarse sand. Similarly, no chemicals reached the groundwater table for groundwater depths deeper than 3 m in silt.

4.2. Cleanup time

4.2.1. Effect of chemical properties and removal mechanisms

Groundwater cleanup times required to remove NAPL mass for the six chemicals are shown in Fig. 8. The chemicals are presented from left to right corresponding to their order of solubility in water. Groundwater cleanup time was inversely proportional to chemical solubility. Three high solubility chemicals, acrylonitrile, MTBE, and vinyl acetate, have solubility greater than 20,000 mg/L (Table 1). As expected, high solubility chemicals easily dissolved into water so the pumping system very effectively removed NAPL. For the three low solubility chemicals, benzene (1750 mg/L), styrene (300 mg/L), and cyclohexane (55 mg/L), the groundwater cleanup time increased (in two cases >75,000 days) dramatically compared to the high solubility chemicals.

For all soil types, the groundwater cleanup time generally decreased with increasing depth to groundwater and decreasing spill volume due to the decrease in NAPL volume across the capillary fringe. The 50% and 90% spill volumes had almost the same cleanup time because the similar infiltration rate (spill volume over spill area) resulted in similar NAPL distributions, except for the width of the NAPL source zone perpendicular to flow. Hence, more pumping wells were required in the 90% case due to its larger spill area. For similar reasons, more pumping wells were also required for the 50% and 90% spill volumes of styrene at 3 m than at 6 m; as a result, the 6 m case took slightly longer time to clean up than the 3 m case (Fig. 8). Cleanup times computed for low solubility chemicals (i.e., benzene, styrene, cyclohexane) are excessive, and thus removal mechanisms for the NAPL form of these chemicals in groundwater are discussed next in order to evaluate other potential remediation strategies besides pump and treat.

We calculated the cumulative mass removal of the NAPL lens as a function of time for the three lowest solubility chemicals for a groundwater depth of 3 m and a 50% spill volume (Fig. 9). The removal time of the NAPL lens was much longer than for the residual NAPL, so only removal of the NAPL lens is discussed here. In coarse sand, mass removal by vertical dispersion is greater than mass removal by advection. Mass removal by advection was low due to reduction of the water relative permeability in the NAPL lens (k_{rw} = 0.037 at S_n = 0.35). In silt, the contribution of dispersion to mass removal decreased compared to coarse sand. This is because the NAPL lens is only 3 m long in the main flow direction in silt, but 20 m long in coarse sand (Eq. (15)).

For the lower solubility chemicals, diffusive flux via vapor transport toward the ground surface (Eq. (16)) becomes a more important mechanism because of the long removal period. For cyclohexane, most of the NAPL mass (>87%) was removed by vapor diffusion due to its high vapor pressure and extremely low solubility; the vapor diffusive flux only became negligible after the portion of the NAPL lens in direct contact with the gas phase was completely removed (Fig. 9(e) and (f)). For benzene, only half the NAPL in the capillary fringe was removed by vapor diffusion due to its higher solubility compared to cyclohexane, resulting in a shorter removal time than for cyclohexane. For styrene, vapor diffusive NAPL removal was low because of its low vapor pressure.

4.2.2. Effect of excavation

Values of NAPL volume that reached groundwater and cleanup times in coarse sand and silt for benzene are shown in Fig. 10 for different excavation scenarios. In coarse sand, faster excavation generally results in less NAPL in groundwater, and the effect is more pronounced at greater groundwater depths. However, the effect is relatively small, compared to that in silt. This is because the infiltration times, relative to excavation time, are shorter in coarse sand than in silt. In coarse sand, less NAPL in groundwater and faster excavation only marginally influenced groundwater cleanup time. This is because the size of the NAPL source zone was only slightly larger with the additional NAPL volume, and the NAPL removal rate due to dispersion was slightly higher. In silt, less NAPL in groundwater results in shorter groundwater cleanup times. Results for fine sand (not shown) were intermediate between coarse sand and silt. These results imply that for low permeability soils like silt, rapid excavation can be very effective at reducing the extent of groundwater contamination and groundwater cleanup times. In Fig. 10 the NAPL amount that reached groundwater was computed at 30 days, but the case with no excavation still has free

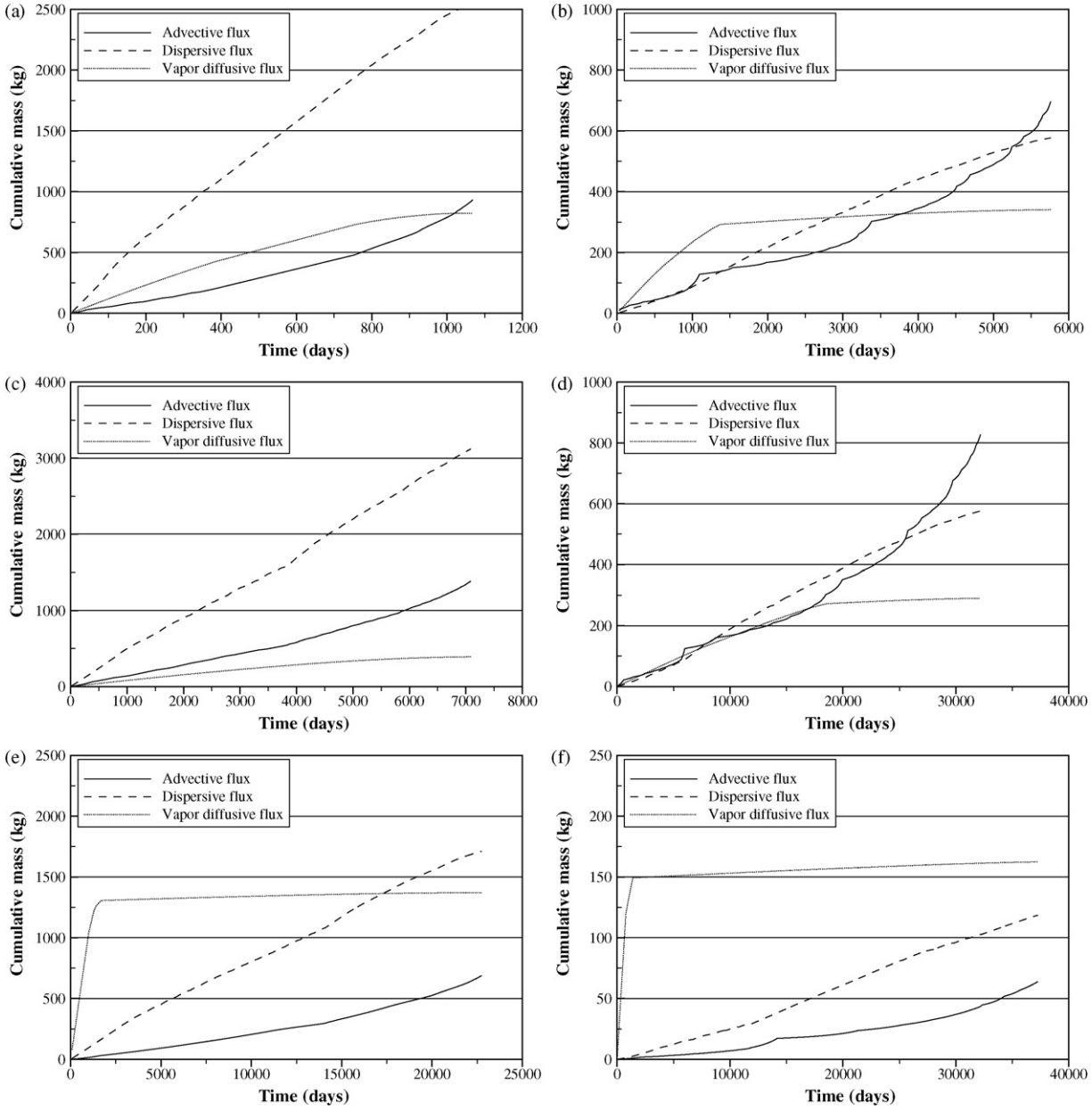

Fig. 9. Cumulative mass removal of the NAPL lens by NAPL dissolution and NAPL volatilization in coarse sand (left) and silt (right) for (a and b) benzene, (c and d) styrene, and (e and f) cyclohexane. The depth to groundwater is 3 m and the spill volume is 50% of a tank car.

NAPL in the vadose zone, which has the potential to cause further contamination.

4.2.3. Effect of free NAPL removal

Groundwater cleanup times for benzene, styrene, and cyclohexane in the three soils with free NAPL removal are shown in Fig. 11. When free NAPL removal is considered, NAPL saturation in the NAPL lens is reduced to a residual NAPL saturation of 0.1 as described previously. For all cases, cleanup times decrease significantly by a factor of 2–7 when free NAPL removal is considered. This is mainly due to the increase in the water relative permeability as NAPL saturations decrease, and the decrease in the total NAPL mass. For example, the water relative permeability increased from 0.037 to 0.6 as the NAPL saturation decreased from 0.35 to 0.1 in coarse sand. Comparison of cleanup times with and without free NAPL removal (Figs. 8 and 11) reveals that the trends in cleanup times as a function of depths to groundwater did not change, but the scale of cleanup times changed for all three chemicals. This is attributed to the assumption that free NAPL removal reduced NAPL saturation, but did not change the size of the NAPL source zone, resulting in similar dispersive fluxes and faster NAPL dissolution by advection.

For 50% and 90% spill cases, cleanup time increased with decreasing soil permeability at the 3 m groundwater depth. In contrast, for 12.5% spill cases, cleanup time did not follow this trend at the same depth. This is because NAPL volume in groundwater in the silt is much smaller than NAPL volume in the sand (Fig. 7), resulting in a longer cleanup time in the sand. Hence, cleanup times in different soils are strongly affected by chemical solubility and diffusion coefficient values in the gas phase as well as NAPL volume in groundwater. In addition, the scale of cleanup time with free NAPL removal for styrene and cyclohexane is still very high because of their low solubilities.

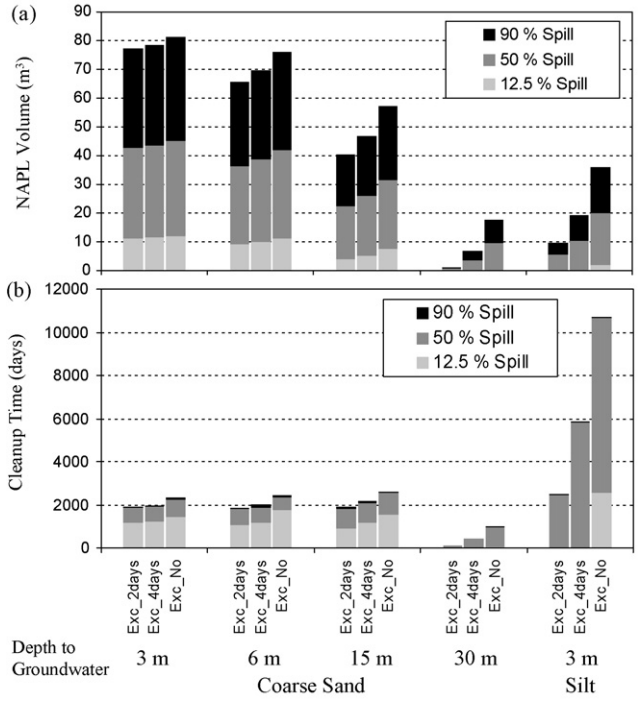

Fig. 10. Effect of excavation on (a) NAPL volume across the capillary fringe and (b) groundwater cleanup time for benzene.

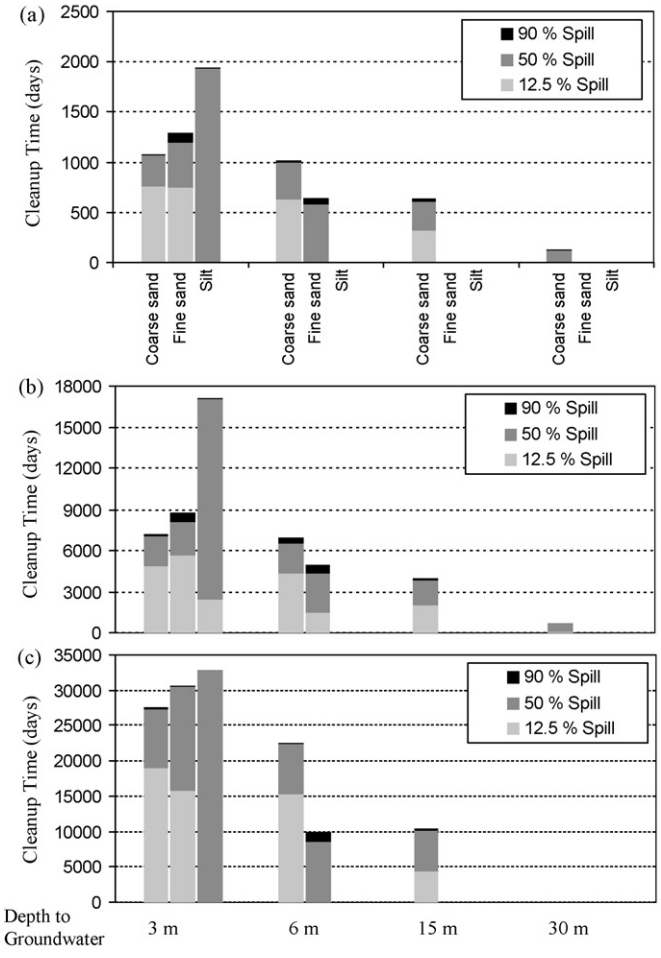

Fig. 11. Groundwater cleanup times with free NAPL removal for (a) benzene, (b) styrene, and (c) cyclohexane.

5. Summary and conclusions

This paper presents a new model that combines modified versions of NAPL infiltration (KOPT-RAIL) and redistribution (OILENS-RAIL) modules in the HSSM, with a new groundwater module. The groundwater module includes source zone removal via NAPL dissolution and volatilization, contaminant plume development via the modified Domenico solution, and the concept of arrival distribution time for a pumping system. The new model is used to assess the influence of NAPL spills for six chemicals on groundwater contamination and remediation with a pumping system. In particular, this study evaluates the effects of chemical properties, soil permeability, spill volume, depth to groundwater, excavation, and free NAPL removal on NAPL volumes that reached groundwater and cleanup times.

(1) In coarse sand, contaminant vapor pressures and density to viscosity ratios were only marginally important in determining NAPL volumes that reached groundwater for shallow groundwater depths. In silt, high vapor pressures (e.g., MTBE) and low density to viscosity ratios (e.g., cyclohexane) had a relatively large impact on NAPL volume across the capillary fringe, because of the slow infiltration time compared to the excavation time of four days. NAPL evaporation into atmosphere caused the net NAPL infiltration rate to decrease and low density to viscosity ratios reduced the NAPL migration rate in the vadose zone. In this study, the infiltration amount for MTBE was reduced by 48% for the 90% spill case in silt, due to NAPL evaporation. Similarly, the excavation time marginally affected the NAPL volume that reached groundwater in sandy soils, but more so in the silt. Hence, shorter excavation times may increasingly reduce the extent of groundwater contamination in lower permeability soils and for chemicals with higher vapor pressures and/or lower density to viscosity ratios.
(2) For high solubility chemicals, the pumping system efficiently removed all NAPLs and captured the contaminant plume relatively quickly (Fig. 7), while for low solubility chemicals, the pumping system was not efficient (Fig. 8). Dispersion from the NAPL source zone (Eq. (15)) controlled the rate of NAPL dissolution. The model results show that the NAPL removal rate by dispersion from the NAPL lens was not fast enough to consider pumping an efficient technology for low solubility chemicals.
(3) For low solubility chemicals, free NAPL removal reduced the cleanup time compared to cases of no free NAPL removal by a factor of 3–15. In contrast to many contaminated sites, chemical spills from railroad-tank-car accidents occur over a short time and the source zone is relatively well characterized. Hence, free NAPL removal is expected to reduce the cleanup time. However, even after free NAPL removal the cleanup times can be very long, in particular for extremely low solubility chemicals like cyclohexane and styrene.

There are several important limitations of the model and our evaluation. After the NAPL lens forms, the NAPL distribution is assumed to be in vertical equilibrium and immobile during pumping. Some free NAPL will be mobilized due to the induced head gradient by a pumping well. Water fluctuation and NAPL volatilization of the NAPL lens will change the vertical equilibrium of the NAPL distribution. Hence, the effects of vertical and horizontal flows could be significant. In the current model, we separately treated the NAPL lens and entrapped NAPL in the vadose zone. As described previously, NAPL in the vadose zone can infiltrate into groundwater before pumping. It was assumed that all remaining NAPL in the vadose zone is removed by soil excavation or soil vapor extraction when pumping begins. Hence, NAPL in the vadose zone is

not considered a long-term source of groundwater contamination after pumping. However, soil vapor extraction can enhance NAPL removal from the lens because the diffusion distance to flowing air flow induced by soil vapor extraction is smaller than the diffusion distance to the ground surface.

A continuous pumping strategy is often not practical, in particular for long periods of cleanup. Like other screening models, subsurface heterogeneity is not accounted for. The effect of the geometry of spill shapes requires further investigation. Source zone natural attenuation (including biodegradation) can be important for many petroleum hydrocarbons for long-term remediation, but is not considered in the model. The source zone natural attenuation approach developed by [48,49] can be incorporated into the current model framework. The model includes functionality for NAPL component degradation in groundwater, but this was not evaluated to facilitate comparison of other removal processes. Finally, incorporation of other remediation technologies such as in-situ air sparging and dynamic free NAPL removal (e.g., bioslurping and multiphase extraction) and coupling vadose zone and groundwater remediation systems may improve the ability of the model to more accurately assess cleanup times for the variety of chemicals shipped in railroad tank cars.

Acknowledgments

This research was sponsored by the Association of American Railroads. The authors are grateful to Robert Fronczak, Chester Culley, David Clark, Geoff Reeder, and Bruce Williams for their support and assistance providing information and data regarding spills of hazardous materials. Thanks also to John Zeman and Neha Hridaya for their help on this project. We also acknowledge the effort of the Reviewers, whose comments have led to significant improvement of our manuscript.

References

[1] BOE, Bureau of Explosives, Annual Report of Hazardous Materials Transported by Rail: Calendar Year 2005, Association of American Railroads, Report BOE 05-1, Pueblo, CO, USA, 2006.
[2] P. Anand, C.P.L. Barkan, A geographic information system analysis of the exposure of soil and groundwater to spills of hazardous materials transported by rail, Transport. Res. Rec.: J. Transport. Res. Board 1943 (2006) 12–19.
[3] C.P.L. Barkan, T.S. Glickman, A.E. Harvey, Benefit-cost evaluation of using different specification tank cars to reduce the risk of transporting environmentally sensitive chemicals, Transport. Res. Rec.: J. Transport. Res. Board 1313 (1991) 33–43.
[4] P. Anand, Cost-effectiveness of reducing environmental risk from railroad tank car transportation of hazardous materials, Ph.D. Dissertation, University of Illinois at Urbana-Champaign, Urbana, IL, USA, 2006.
[5] ERS, Environmental Risk Sciences, Inc., Reference manual for the evaluation of the environmental hazards of chemicals, InterIndustry Rail Safety Task Force (IIRSTF), Washington, DC, USA, 1994.
[6] C.T. Miller, G. Christakos, P.T. Imhoff, J.F. McBride, J.A. Pedit, J.A. Trangenstein, Multiphase flow and transport modeling in heterogeneous porous media: challenges and approaches, Adv. Water Res. 21 (2) (1998) 77–120.
[7] L.M. Abriola, J. Lang, K. Rathfelder, Michigan Soil Vapor Extraction Remediation (MISER) Model—A Computer Program to Model Bioventing of Organic Chemicals in Unsaturated Geological Material, EPA/600/R-97/099, U.S. EPA, Cincinnati, OH, USA, 1997.
[8] M.D. White, M. Oostrom, STOMP, Subsurface Transport Over Multiple Phases, Version 2.0 Theory Guide, PNNL-12030 Pacific Northwest National Lab., Richland, WA, USA, 2000.
[9] M.D. White, M. Oostrom, STOMP, Subsurface Transport Over Multiple Phases, Version 3.1 User's Guide, PNNL-14478 Pacific Northwest National Lab., Richland, WA, USA, 2004.
[10] K. Pruess, A. Battistelli, TMVOC, a Numerical Simulator for Three-Phase Non-Isothermal Flows of Multicomponent Hydrocarbon Mixtures in Saturated-Unsaturated Heterogeneous Media, LBNL-49375 Lawrence Berkeley National Lab., Berkeley, CA, USA, 2002.
[11] K. Pruess, C. Oldenburg, G. Moridis, TOUGH2 User's Guide, Version 2.0, LBNL-43134 Lawrence Berkeley National Lab., Berkeley, CA, USA, 1999.
[12] University of Texas at Austin, Technical documentation for UTCHEM-9.0: a three-dimensional chemical flood simulator, reservoir engineering research program, center for petroleum and geosystems engineering, University of Texas at Austin, TX, USA, 2000.
[13] V. Ravi, J.R. Williams, Estimation of Infiltration Rate in the Vadose Zone: Compilation of Simple Mathematical Models EPA/600/R-97/128a, U.S. EPA, Ada, OK, USA, 1998.
[14] J.W. Weaver, R.J. Charbeneau, B.K. Lien, A screening model for nonaqueous phase liquid transport in the vadose zone using Green–Ampt and kinematic wave theory, Water Resour. Res. 30 (1) (1994) 93–105.
[15] J.W. Weaver, R.J. Charbeneau, J.D. Tauxe, B.K. Lien, J.B. Provost, The Hydrocarbon Spill Screening Model (HSSM) Volume 1: User's Guide, EPA/600/R-94/039a, 1994.
[16] R.J. Charbeneau, J.W. Weaver, B.K. Lien, The Hydrocarbon Spill Screening Model (HSSM) Volume 2: Theoretical Background and Source Codes, EPA/600/R-94/039b, 1995.
[17] J.W. Weaver, Application of the hydrocarbon spill screening model to field sites, in: L.N. Reddi (Ed.), Non-Aqueous Phase Liquids (NAPLs) in Subsurface Environment: Assessment and Remediation, American Society of Civil Engineers, New York, USA, 1996, pp. 788–799.
[18] C. Eberhardt, P. Grathwohl, Time scales of pollutants dissolution from complex organic mixtures: blobs and pools, J. Contam. Hydrol. 59 (1–2) (2002) 45–66.
[19] D. Huntley, G.D. Beckett, Persistence of LNAPL source: relationship between risk reduction and LNAPL recovery, J. Contam. Hydrol. 59 (2002) 3–26.
[20] R.W. Falta, Modeling sub-grid-block-scale dense nonaqueous phase liquid (DNAPL) pool dissolution using a dual-domain approach, Water Resour. Res. 39 (12) (2003) 1360.
[21] T.P. Chan, S. Rao, Govindaraju, stochastic-advective transport model for NAPL dissolution and degradation in non-uniform flows in porous media, J. Contam. Hydrol. 87 (3–4) (2006) 253–276.
[22] U. Maier, P. Grathwohl, Numerical experiments and field results on the size of steady state plumes, J. Contam. Hydrol. 85 (2006) 33–52.
[23] E.A. Seagren, B.E. Rittman, A.J. Valocchi, A critical evaluation of the local-equilibrium assumption in modeling of NAPL-pool dissolution, J. Contam. Hydrol. 39 (1999) 109–135.
[24] P.I. Kawamura, D. Mackay, The evaporation of volatile liquids, J. Hazard. Mater. 15 (1987) 343–364.
[25] D. MacKay, R.S. Matsugu, Evaporation rate of hydrocarbon spills on water and land, Can. J. Chem. Eng. 5 (1973) 434–439.
[26] M. Hussein, M. Jin, J.W. Weaver, Development and verification of a screening model for surface spreading of petroleum, J. Contam. Hydrol. 57 (3–4) (2002) 281–302.
[27] R.J. Lenhard, M. Oostrom, J.H. Dane, A constitutive model for air-NAPL-water flow in the vadose zone accounting for residual NAPL in strongly water-wet porous media, J. Contam. Hydrol. 73 (1–4) (2004) 281–304.
[28] R.H. Brooks, A.T. Corey, Hydraulic Properties of Porous Media: Hydrology Papers, Colorado State University, CO, USA, 1964.
[29] J. Bear, Hydraulics of Groundwater, McGraw-Hill, NY, USA, 1979.
[30] M. Oostrom, J.H. Dane, T.W. Wietsma, A review of multidimensional, multifluid intermediate-scale experiments: Nonaqueous Phase Liquid dissolution and enhanced remediation, Vadose Zone J. 5 (2006) 570–598.
[31] J.R. Hunt, N. Sitar, K.S. Udell, Non-aqueous phase liquid transport and cleanup: analysis of mechanisms, Water Resour. Res. 24 (8) (1988) 1247–1258.
[32] C. Zhang, H. Yoon, C.J. Werth, A.J. Valocchi, N.B. Basu, J.W. Jawitz, Evaluation of simplified mass transfer models to simulate the impacts of source zone architecture on Nonaqueous Phase Liquid dissolution in heterogeneous porous media, J. Contam. Hydrol. 102 (1–2) (2008) 48–59, doi:10.1016/j.jconhyd.2008.05.007.
[33] R. Millington, J. Quirk, Permeability of porous solids, Trans. Faraday Soc. 57 (1961) 1200–1207.
[34] P.A. Domenico, An analytical model for multidimensional transport of a decaying contaminant species, J. Hydrol. 91 (1987) 49–58.
[35] J.M. Martin-Hayden, G.A. Robbins, Plume distortion and apparent attenuation due to concentration averaging in monitoring wells, Ground Water 35 (2) (1997) 339–346.
[36] C.E. Aziz, C.J. Newell, J.R. Gonzales, P. Haas, T.P. Clement, Y-W. Sun, BIOCHLOR Version 1.0 User's Manual, EPA/600/R-00/008, U.S. EPA, Ada, OK, USA, 2000.
[37] E. Wexler, Analytical solutions for one-, two-, and three-dimensional solute transport in groundwater systems with uniform flow, USGS-TWRI Book 3, Chap. B7, 1992.
[38] V. Srinivasan, T.P. Clement, K.K. Lee, Domenico solution—is it valid? Ground Water 45 (2) (2007) 136–146.
[39] M.R. West, B.H. Kueper, M.J. Ungs, On the use and error of approximation in the Domenico (1987) solution, Ground Water 45 (2) (2007) 126–135.
[40] M. Karanovic, C.J. Neville, C.B. Andrews, BIOSCREEN-AT: BIOSCREEN with an exact analytical solution, Ground Water 45 (2) (2007) 242–245.
[41] S. Grubb, Analytical model for estimation of steady-state capture zones of pumping wells in confined and unconfined aquifers, Ground Water 31 (1) (1993) 27–32.
[42] M.J. Simpson, Computing residence times for flow towards a pumping well: nomograph solution and validity of the small draw-down approximation, Hydrogeol. J. 13 (2005) 889–894.
[43] J. Bear, M. Jacob, On the movement of water bodies injected into aquifers, J. Hydrol. 3 (1965) 37–57.
[44] R. Nelson, Evaluating the environmental consequences of groundwater contamination, Water Resour. Res. 14 (3) (1978) 409–450.

[45] W. Kinzelbach, Groundwater Modelling, Elsevier Science Publishers, New York, USA, 1986.
[46] P. Anand, Quantitative assessment of the exposure of environmental characteristics to railroad spills of hazardous materials, Master's Thesis, University of Illinois at Urbana-Champaign, Urbana, IL, USA, 2004.
[47] T.T. Treichel, J.P. Hughes, C.P.L. Barkan, R.D. Sims, E.A. Phillips, M.R. Saat, Y.K. Wen, D.G. Simpson, Safety Performance of Tank Cars in Accidents: Probabilities of Lading Loss (RA-05-02) RSI-AAR Railroad Tank Car Safety Research and Test Project, Leesburg, VA, USA, 2006.
[48] P.C. Johnson, P.D. Lundegard, Z. Liu, Source zone natural attenuation at petroleum hydrocarbon spill sites—I: site-specific assessment approach, Ground Water Monit. Remediation 26 (4) (2006) 82–91.
[49] P.D. Lundegard, P.C. Johnson, Source zone natural attenuation at petroleum hydrocarbon spill sites—II: Application to source zones at a former oil production field, Ground Water Monit. Remediation 26 (4) (2006) 93–106.
[50] U.S. NLM, Hazardous Substances Data Banks (HSDB), U.S. National Library of Medicines, Available online at http://toxnet.nlm.nih.gov.
[51] A.H. Demond, A.L. Lindner, Estimation of interfacial tension between organic liquids and water, Environ. Sci. Technol. 27 (12) (1993) 2318–2331.
[52] U.S. EPA, Industrial waste management evaluation model (IWEM) technical background document, EPA530-R-02-012, Office of Solid Waste and Emergency Response (5305W), Washington, DC, USA, 2002.
[53] S. Ohe, Computer aided data book of vapor pressure, Data Book Publishing Inc., Tokyo, Japan, 1976, Available online at http://www.s-ohe.com/Acetonitrile_cal.html.
[54] A. Hickel, C.J. Radke, H.W. Blanch, Role of organic solvents on Pa-hydroxynitrile lyase interfacial activity and stability, Biotechnol. Bioeng. 74 (1) (2001) 18–28.